Structural Engineering and Mechanics, Vol. 16, No. 4 (2003) 405-422
DOI: http://dx.doi.org/10.12989/sem.2003.16.4.405

Energy dissipation response of brick masonry under cyclic compressive loading

R. Senthivel† and S. N. Sinha‡

Department of Civil Engineering, Indian Institute of Technology, Delhi - 110016, India

(Received August 12, 2002, Accepted April 16, 2003)

Abstract. Scaled brick masonry panels were tested under cyclic unialxial compression loading to evaluate its deformation characteristics. An envelope stress - strain curves, a common point curves and stability point curves were obtained for various cyclic test conditions. Loops of the stress-strain hysteresis were used to determine the energy dissipation for each cycle. Empirical expressions were proposed for the relations between energy dissipation and envelope and residual strains. These relations indicated that the decay of masonry strength starts at about two-third of peak stress.

Key words: brick; uniaxial; envelope curve; common point; stability point; cyclic loading; Stress-Strain Hysteresis; energy dissipation; envelope strain; plastic strain.

1. Introduction

Numerous studies have been made on the behaviour of brick masonry under monotonically increasing load (e.g., Atkinson *et al*. 1983, Khoo *et al*. 1973, Warren *et al*. 1981). Most studies on masonry under cyclic loading have been mainly directed at the objective of earthquake resistant design of masonry buildings (e.g., Mayes *et al*. 1975, Mengi *et al*. 1989, Shing *et al*. 1987). Limited studies have been performed on the behaviour of brick masonry under uniaxial compressive or uniaxial tensile cyclic loading. Cyclic loading tests on brick masonry provide vital information related to material's ductility, stiffness degradation and energy dissipation characteristics. The deformation characteristics of brick masonry under repeated or reversed cyclic loading have been evaluated only during the last decade (Naraine and Sinha 1989). The effect of repeated compressive loading is particularly relevant to brick masonry structures having a large live load to dead load ratio.

Cumulative energy dissipation is often used as a measure of the seismic performance of a structure. The performance of reinforced concrete structures is widely quantified on the basis of the concept of energy dissipation (Bertero *et al*. 1977, Darwin and Nmai 1986, Hwang and Scibner 1984). Low energy dissipation characterises the brittle behaviour of the structure while high energy dissipation indicates a ductile behaviour. Energy dissipation capacity has been used to assess the ability of a structural member to withstand cyclic loading in the inelastic range and serves as an

† Ph. D. Scholar
‡ Professor & Chair

indicator of the member's capability to sustain damage without collapse (Banon *et al*. 1981, Gosain *et al*. 1977, Popov 1968). Energy dissipation, usually expressed as a non-dimensional ratio (Chen *et al*. 1978, Hidalgo 1978) is defined as the energy dissipated per cycle to the total input energy. The test results indicate that the energy dissipation ratio, R_n increases linearly as a function of the imposed displacement at early loading stage. Upon the onset of cracking, the energy dissipation ratio shows a significant increase due to further increase in displacement.

The objective of the present study was to establish the non-linear stress - strain characteristics of calcium silicate brick masonry under repeated compressive loading. Since brick masonry exhibits distinct directional properties, the study is made for calcium silicate brick masonry with five different bed joint orientations comprising 0^o, 22.5^o, 45^o, 67.5^o and 90^o to the loading direction. An attempt was made to establish envelope stress - strain curves, common point stress - strain curves and stability point stress - strain curves for these bed joint inclinations. Loops of the stress-strain hysteresis were used to determine the energy dissipation for each cycle. Empirical expressions were proposed for the relations between energy dissipation and envelope and residual strains.

2. Experimental program

2.1 Test specimens

A full-scale solid calcium silicate brick unit measures 230 mm × 110 mm × 70 mm. Eight half-scale brick units measuring 110 mm × 55 mm × 35 mm were sawn out from each full brick. Based on a sample of 30 single unit bricks, the average compressive strength of half-scale brick was found to be 24.3 MPa. A 1:1/2:4 mix by volume of cement, lime and sand with a Water/Cement ratio of 0.95 by weight was used for mortar. The average compressive strength of mortar was observed to be 10.6 MPa at 28 days on testing a sample of 30 mortar cubes with 70 mm dimension. Seventy-five English bond panels with 5 mm thick mortar joints were fabricated with varying bed joint inclinations by cutting individual bricks to the shape required. The dimensions of the test panel were adopted as 360 mm × 360 mm × 115 mm. The details of test panel are as shown in Fig. 1. In order to maintain uniform workmanship, all test specimens were constructed by the same mason. Brick

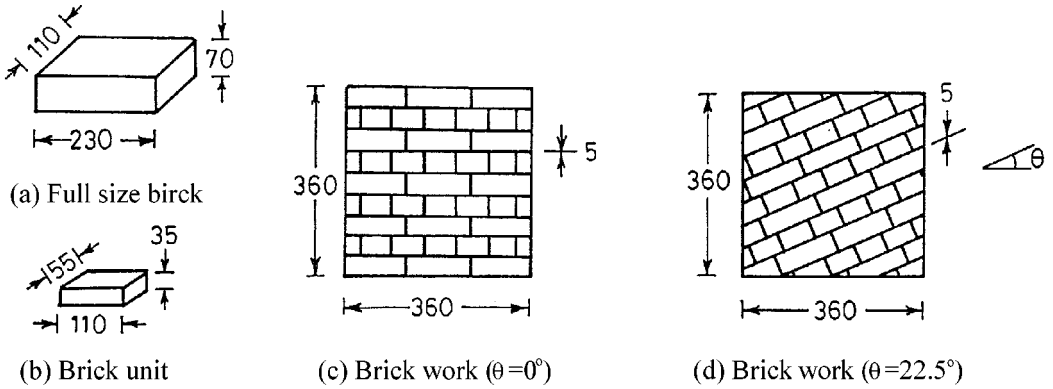

All dimensions in mm

Fig. 1 Details of test panels

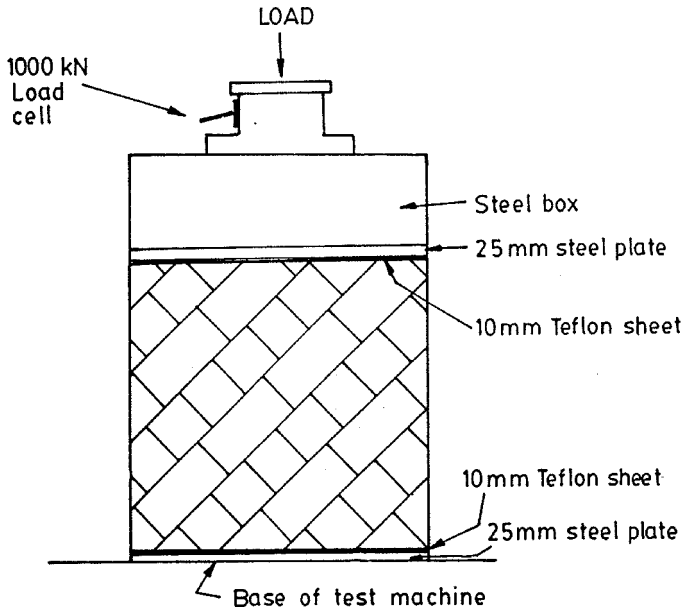

Fig. 2 Compression test set-up

units were first soaked in water for about 5 minutes and then left to dry for another 15 minutes before being laid for panel construction. Thereafter, the panels were cured by covering them with wet jute sacks for 28 days. Immediately after construction the panels were subjected to a small weight of about 12 Kg for twenty four hours to ensure bond between brick units and bed mortar joints particularly for the upper most courses.

2.2 Loading arrangements

The calcium silicate brick masonry panels were tested in compression and tension using an Avery Universal Testing Machine (UTM) of 1000 KN capacity. For compression test, the load was distributed through a steel box of 150 mm × 200 mm cross-section. A load cell of 1000 KN capacity was placed between the testing machine and the steel box at its centre as shown in Fig. 2.

2.3 Instrumentation

The masonry panels were instrumented with LVDTs (Linearly Variable Displacement Transducers) aligned in mutually orthogonal directions on both sides of the panel. The arrangement of LVDTs and loading directions are shown in Fig. 3. The LVDTs were installed to measure the axial and lateral displacement over a fixed gauge length. A gauge length of 250 mm was adopted for measurement of both axial and lateral deformations. A Pentium based Data Acquisition and Control Software System was used to display monitor and record the load and displacement measurements in real time. The axial displacement at the two locations on each side of the panel were plotted versus load in real time during the test. The plots of axial displacement versus lateral displacement were also obtained at the same locations.

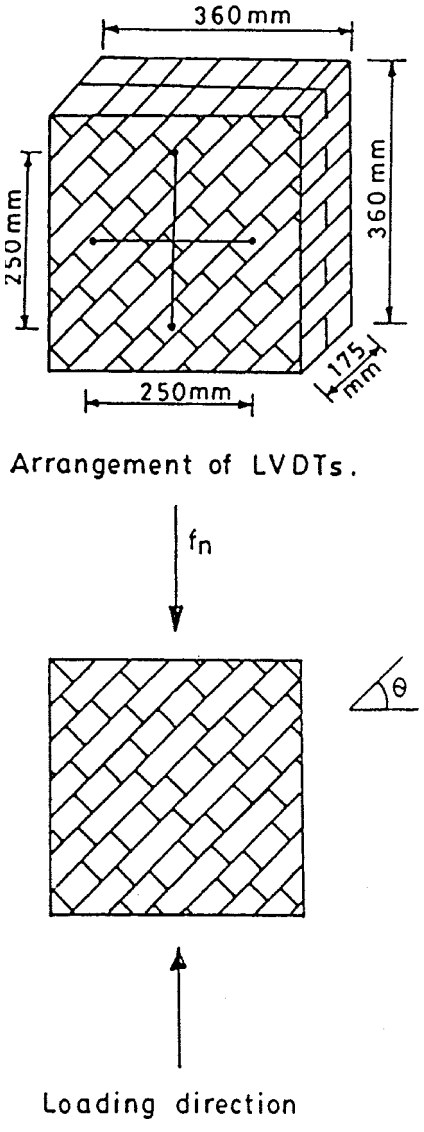

Fig. 3 LVDTs arrangement and loading direction

2.4 Test procedures

Three types of test (Test types I, II and III) were conducted for each of the selected bed joint inclination i.e., 0^o, 22.5^o, 45^o, 67.5^o and 90^o to the horizontal.

Test Type I (Envelope test): A monotonic uniaxial loading test, in which load was steadily increased to failure for obtaining the monotonic stress - strain curve. Three specimens were tested for each selected bed joint inclinations.

Test Type II (Common point test): A cyclic uniaxial loading test in which the peak stress achieved in each cycle of loading approximately coincided with the peak stress observed in the monotonic

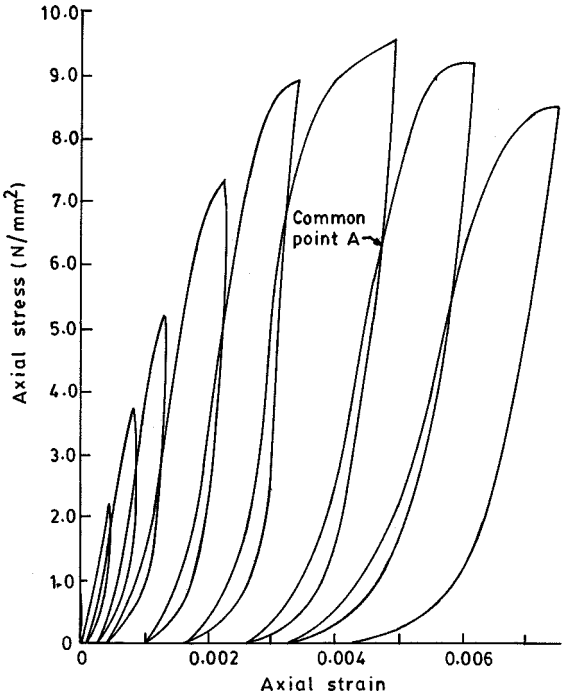

Fig. 4 Typical stress-strain hysteresis curve under cyclic compressive loading (Common Point Test)

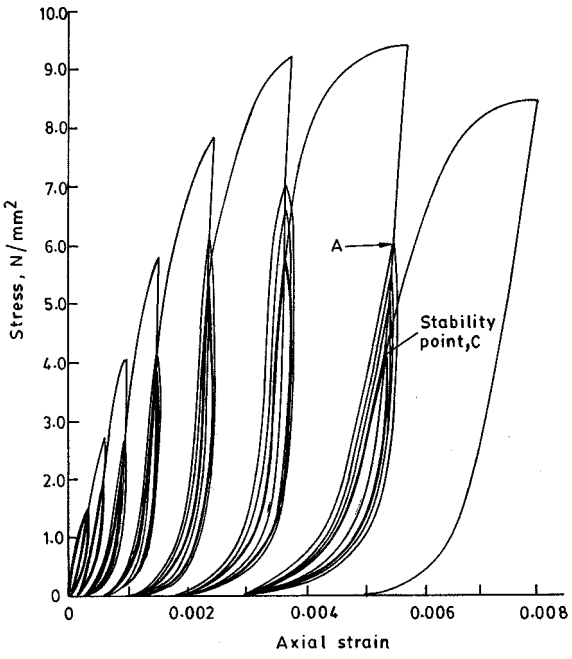

Fig. 5 Typical stress-strain hysteresis curve under cyclic compressive loading (Stability Point Test)

loading. In the ascending zone of the stress - strain curve, the load histories were controlled by monitoring and adjusting the incremental strain increase in each cycle. An incremental strain increase of $0.2 \times 10^3 - 0.5 \times 10^3$ in each cycle was found to be appropriate for the reloading curve to coincide with the envelope curve. In the descending zone, the load was released when reloading curve displayed an impending descent. Three specimens were tested for each of the selected bed joint inclinations.

Test Type III (Stability point test): A cyclic uniaxial loading test as in case of test type II with the exception that unloading and reloading was repeated several times in each cycle of loading. The unloading was initiated when the reloading curve intersected the previous unloading curve until the intersection points of further cyclic curves coincide with the previous intersection point. Four specimens were tested for each selected bed joint orientation.

In test type II, the stress - strain hysteresis generated a locus formed by points of intersection of the loading and unloading curves. Such points of intersection are termed as the common points and may be tracked to identify as locus. A common point may be defined as the point at which the reloading curve of any cycle crosses the unloading curve of the previous cycle (e.g. point A on Fig. 4). In test type III, each time loading-unloading sequence was repeated in any cycle, another common point was observed at a lower position than that of the previous one. Thus, a locus of common points formed with a progressively descending trend as the loading-unloading cycle is repeated, until the locus of common points stabilises at a lower bound (e.g. point C in Fig. 5). Further cycling after

the formation of point C produced a closed hysteresis loop. The locus of these lower bound points are termed stability points.

In the monotonic loading test, the loads were increased steadily at an uniform rate such that the failure of the specimen was achieved at 2.5 to 3 minutes from the start of loading. In the cyclic tests, the loading was applied at a stress rate of about 3.0 N/mm^2 per minute and released at a stress rate of about 6.0 N/mm^2 per minute.

Test type I was successfully completed for bed joint inclinations of 45^o and 67.5^o and Test types II and III could not performed due to extremely small deformations measured under the application of load that did not result in any distinct pattern amidst the regular noise in the signal.

3. Test results and evaluation

3.1 Failure mode

The normal stresses at the bed joints were observed to be compressive in direction for all bed joint orientations in case of the uniaxial compression testing. The failure modes of the panels depended on the ratio of shear stress to normal stress at the bed joints. For high ratios (low normal stress), failure occurred as a bond failure in one of the bed joints with no sign of distress in the bricks. For low ratios (high normal stress), a combined brick-mortar failure was observed. A lateral tensile splitting was evident in the brick with some bond failure in the joints. The higher load capacity of the panels in the latter case may be attributed to the additional frictional resistance in the joint due to the normal compressive stress.

When loaded perpendicular to the bed joints (θ = 0^o), the panels displayed a typical mode of failure due to splitting of bricks through vertical plane and splitting of the face joints, induced by the disparate stress-strain characteristics of the weaker mortar and the stronger bricks. Numerous micro-cracks developed parallel to the direction of the applied load. The eventual collapse of the panels was precipitated by widening of some of these micro -cracks into few major cracks. The test specimens with bed joint angles of 45^o and 67.5^o to the horizontal displayed a failure pattern that was confined to the joints, whereas the specimens with bed joint inclination of 22.5^o to the horizontal exhibited a failure mode similar to that observed in case of bed joint orientation of 0^o (i.e. normal compression). In the case of θ equals to 22.5^o, however, partial bond failures in the joints were accompanied by splitting of bricks. In case of the test specimens with bed joint inclination of 90^o to the horizontal, the load acted parallel to the bed joints resulting in a failure due to splitting of the panel along the vertical face joints. The splitting initiates at free edges and gradually propagates towards the center of the panel. Thereafter, the thus separated fragments of the panel behave like individual compression members. In case of test panels bed joint angles of 0^o and 90^o, spalling of brick and mortar particles from the panel surfaces revealed a tri-axial state of stress in the brickwork even though the panels were subjected to uniaxial compression. The observed modes of failure for different bed joint inclinations are shown in Fig. 6.

The mean vertical compressive stress at failure (mean compressive strength) of specimens were 9.75 N/mm^2, 7.85 N/mm^2, 1.95 N/mm^2, 1.1 N/mm^2 and 8.175 N/mm^2 for bed joint inclinations of 0^o, 22.5^o, 45^o, 67.5^o and 90^o to the horizontal respectively. The relative measures of the mean compressive strength for the various bed joint inclinations are presented in a non-dimensional form in Fig. 7.

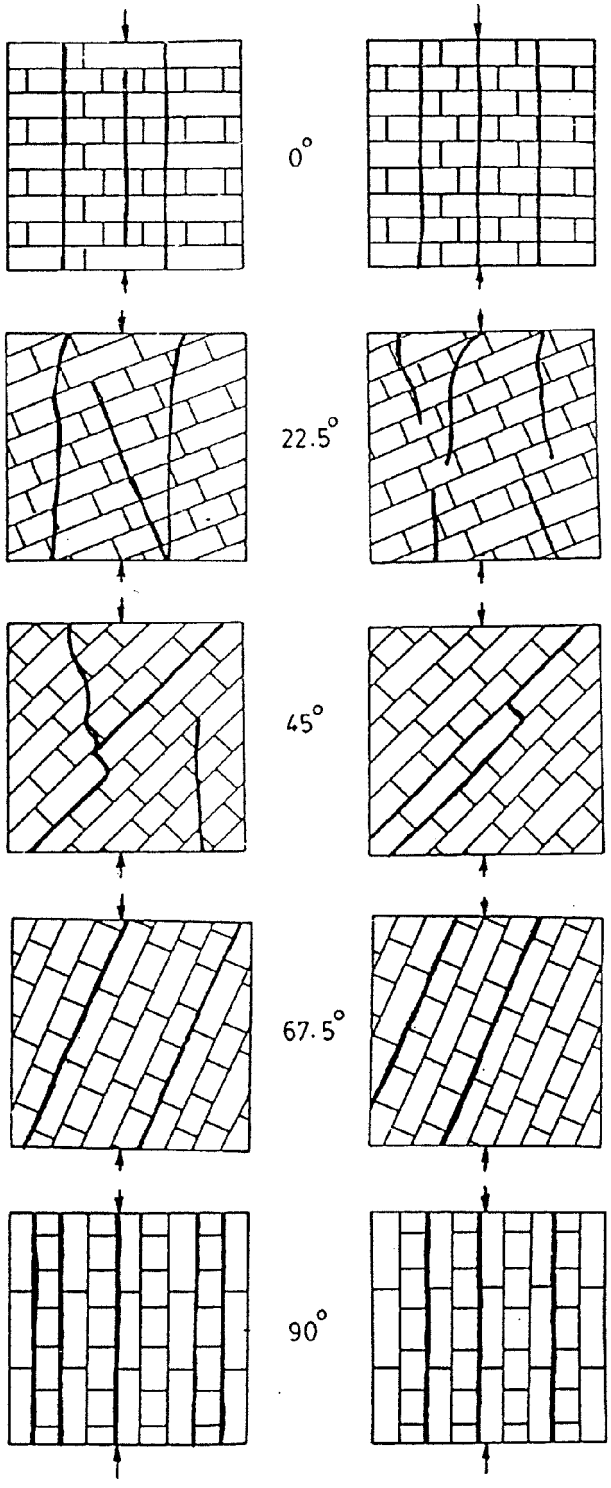

Fig. 6 Modes of failure under compression

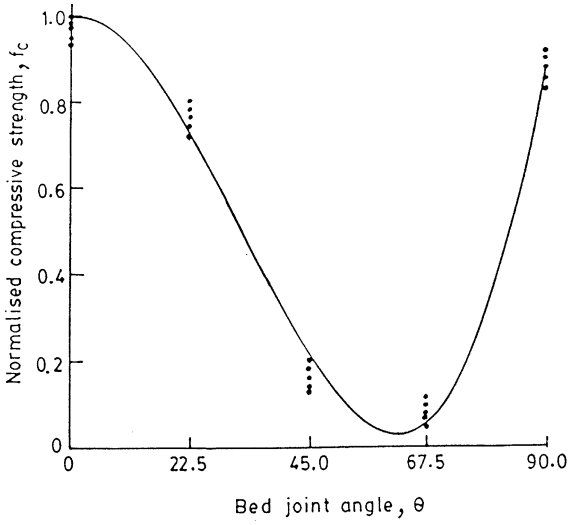

Fig. 7 Influence of bed joint orientation on compressive strength

3.2 Stress - Strain Curve

3.2.1 Envelope curves

The peak points of the hysteretic stress - strain curves under repeated cyclic loading in test types II and III were found to lie on the stress - strain curve under monotonic loading. The stress - strain envelope curve was, therefore, obtained by superposition of the peaks of cyclic stress - strain curves on the monotonic stress strain curve, both are plotted in a non-dimensional coordinate system. The stress coordinate is normalised with respect to the failure (peak) stress, f_m, of each specimen while the strain coordinate is normalised with respect to e_m, the axial strain at which the peak stress is attained. The mean values of strain, e_m were observed as 5.2×10^3, 4.12×10^3, 1.76×10^3, 0.72×10^3 and 5.7×10^3 for bed joint inclination equals to 0^o, 22.5^o, 45^o, 67.5^o and 90^o to the horizontal respectively.

3.2.2 Common point and stability point curves

Test type I was found possible to perform for all bed joint inclinations considered. Test type II and III could not be proceeded for bed joint inclination equals to 45^o and 67.5^o as the deformation under cyclic load was extremely small. For bed joint inclinations of 0^o, 22.5^o and 90^o, the common point under uniaxial cyclic compression were obtained from analysis of data from test types II and III, while the stability points were derived of test type III. These are plotted on a non-dimensional coordinate system.

Based on the experimental data collected by testing the various brick panel specimens under uniaxial cyclic compression and tension, a Polynomial formulation was proposed for envelope, common point and stability point curves, as follows:

$$\sigma = a\varepsilon^4 + b\varepsilon^3 + c\varepsilon^2 + d\varepsilon \qquad (1)$$

Table 1 Values for *a*, *b*, *c*, *d*, and i_c for envelope, common point and stability points curves

Stress-Strain Curves	Bed Joint Angle (θ)	Equation parameters				Correlation coefficient (i_c)
		a	*b*	*c*	*d*	
Envelope curves	0°	–0.1550	0.9584	–2.4003	2.589	0.983
	22.5°	–0.1582	0.8121	–2.088	2.4245	0.9805
	45°	–1.6195	–4.1282	–4.347	2.8342	0.986
	67.5°	–0.867	1.3751	–1.1177	1.614	0.9728
	90°	–0.0151	0.0698	–1.0499	1.9789	0.9719
Common point curves	0°	0.8231	–2.0845	0.3434	1.621	0.9509
	22.5°	0.857	–2.1751	0.4099	1.6079	0.9543
	45°	--	--	--	--	--
	67.5°	--	--	--	--	--
	90°	0.4528	–1.0615	–1.0615	1.9072	0.9481
Stability point curves	0°	1.4169	-3.4035	1.1162	1.3811	0.9583
	22.5°	1.8524	-4.2016	1.5097	1.3253	0.9561
	45°	--	--	--	--	--
	67.5°	--	--	--	--	--
	90°	1.7925	-3.7563	0.8871	1.5356	0.9486

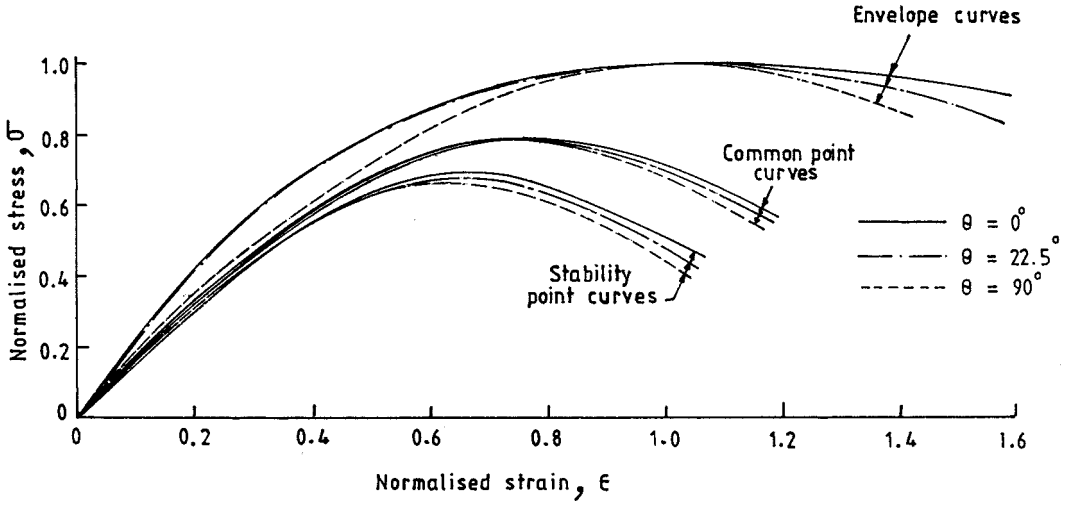

Fig. 8 Normalized stress-strain curves

where,

σ = normalised stress ratio, f/f_m

ε = normalised strain ratio, e/e_m

a, *b*, *c* and *d* = equation's parameters.

For each analytical curve, the values of equation's parameters can be determined from the related data which are presented in Table 1.

The analytical curves of Eq. (1) are drawn along with the corresponding experimental data in Fig. 8.

The degree of fit of each analytical curve with the corresponding experimental data is measured with the coefficient of variation (i_c), which is given in Table 1. It can be observed that the values of i_c ranges from 0.983 to 0.9481. This implies a reasonable degree of fit between the analytical curves and the test data.

3.3 Plastic strain variations

Plastic (residual) strains accumulate with increase in the number and intensity of loading cycles. Fig. 9 displays the plot of the plastic strain at the end of unloading, ε_r with respect to the envelope

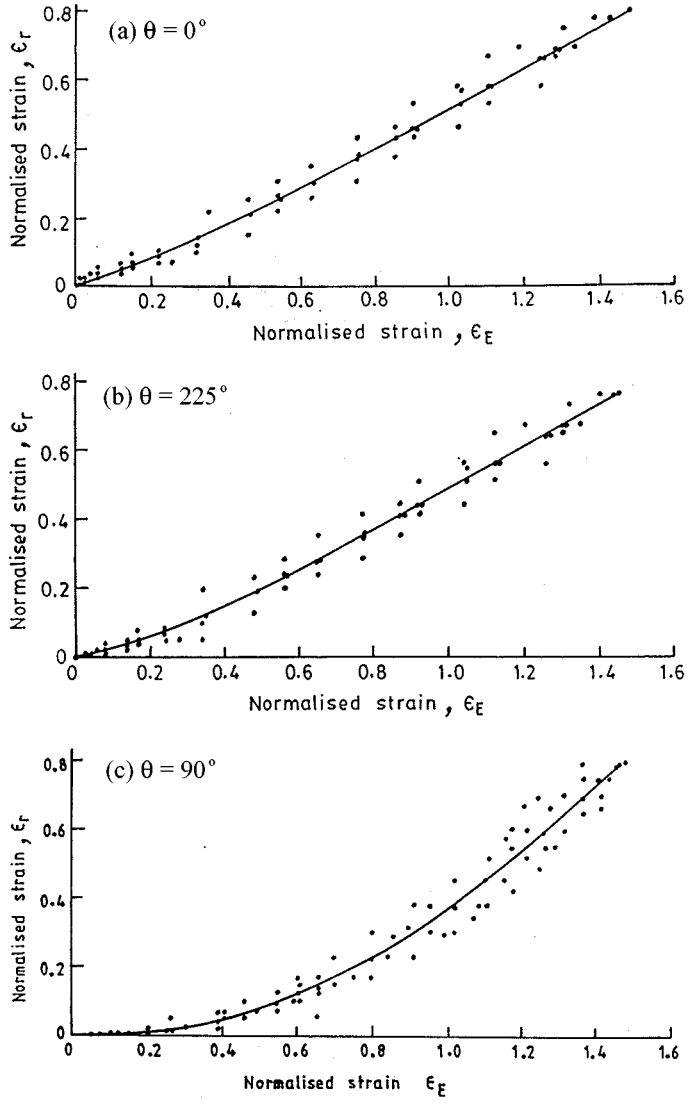

Fig. 9(a, b, c) Variation of envelope strain with plastic strain

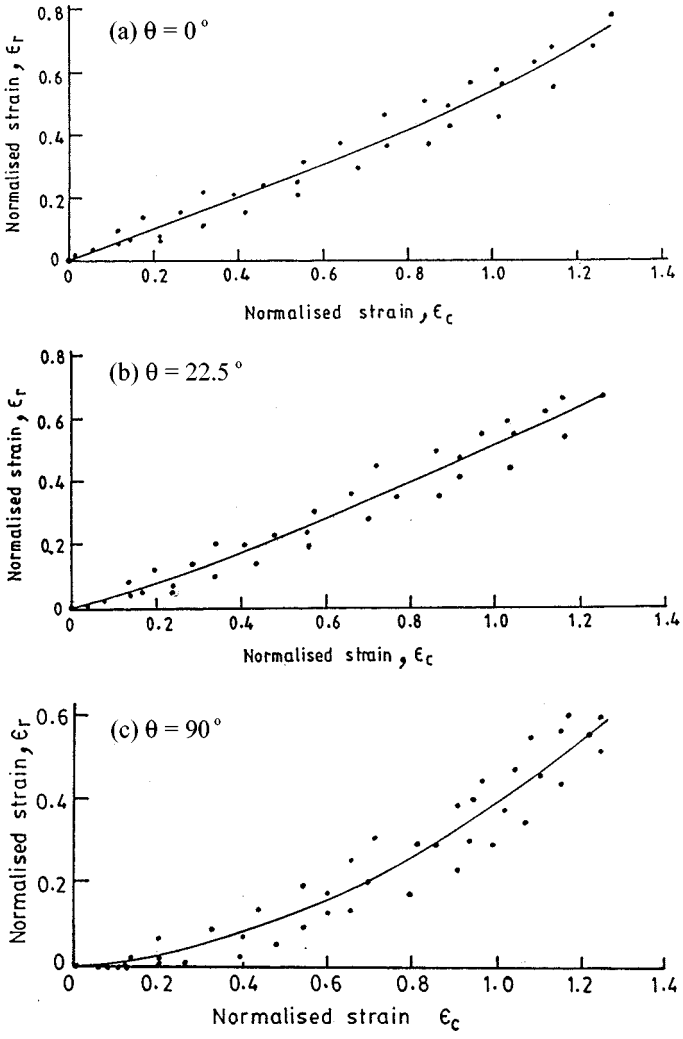

Fig. 10(a, b, c) Variation of common point strain with plastic strain

strain at the beginning of unloading, ε_E for the three loading cases. The variation of ε_r versus ε_E is presented in a non - dimensional coordinate system in Fig. 9. The plastic strain and envelope strain are each normalised with respect to e_m, the strain corresponding to peak stress. The variation of non - dimensional plastic strain at the end of unloading with respect to the non - dimensional strain at common point ε_c as well the non - dimensional strain at stability point ε_s are plotted in Figs. 10 and 11 respectively.

Based on test data, the variations of ε_r versus ε_E, ε_c and ε_s can be modelled by a general polynomial equation with single variable term as follows.

$$\varepsilon_r = a\varepsilon^4 + b\varepsilon^3 + c\varepsilon^2 + d\varepsilon \tag{2}$$

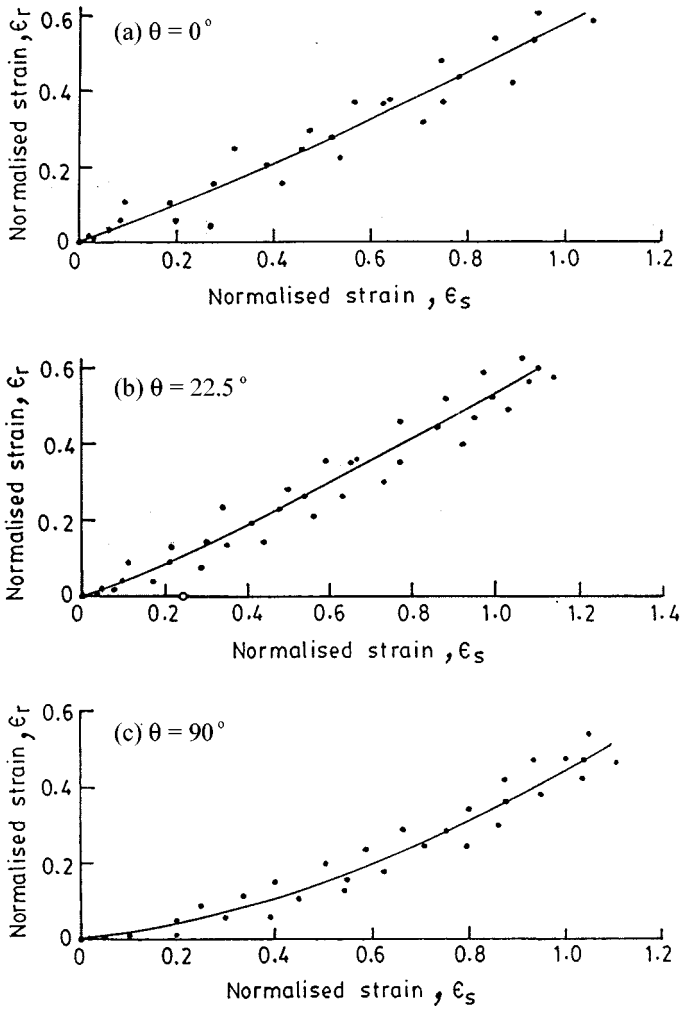

Fig. 11(a, b, c) Variation of stability point strain with plastic strain

Table 2 Values for equations parameters for variation of envelope, common point and stability point strain with plastic strain

Curves		ε_e vs ε_r			ε_c vs ε_r			ε_s vs ε_r		
Bed joint inclination (θ)		0°	22.5°	90°	0°	22.5°	90°	0°	22.5°	90°
Equation parameters	A	0.1262	–0.032	–0.218	0.0669	0.0303	–0.0176	–0.0361	–0.1136	–0.0272
	b	–0.4755	0.023	0.5905	00.2686	–0.0056	0.0153	–0.0482	0.2299	–0.1222
	c	0.6705	0.1421	–0.0841	0.4158	0.0113	0.3416	0.2481	–0.0577	0.5378
	d	0.1697	0.3839	0.0789	0.3004	0.4921	0.0496	0.3736	0.5134	0.0439
	i_c	0.9816	0.9827	0.9685	0.9592	0.9621	0.9354	0.9496	0.9515	0.9582

where,

ε_r = normalised plastic strain

ε = normalised strain at envelope, ε_E, common point, ε_c or stability point, ε_s

a, b, c and d = equation parameters

The values for the constant, a, b, c and d which are determined from the experimental data, depend on stress level and bed joint angles. The values of equation parameters are presented in Table 2.

3.4 Energy dissipation

The energy dissipation ratio, R_n is defined as the ratio of the energy dissipated per cycle to the total input energy as it is illustrated qualitatively in Fig. 12 for a typical reloading - unloading cycle. The energy dissipated per cycle is measured by the area enclosed in the reloading - unloading loop of that cycle. The total input energy per cycle is the total stored strain energy per cycle of reloading - unloading. The area under the curves can be calculated by averaging the readings of a digital planimeter. Fig. 13 shows the plot of the average area against the normalised envelope strain at the peak of each cycle for the three loading cases. A mathematical expression was representing the correlation shown by the plot in Fig. 13 by best fitting the experimental data. The semi - emperical expression can be written in the following general form:

$$R_n = \beta_1 \ln(\varepsilon_E^{\alpha_1} + 1) \tag{3}$$

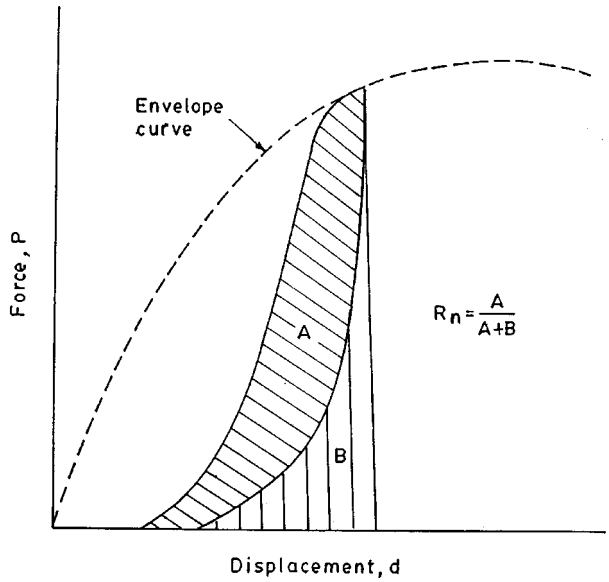

Fig. 12 Determination of R_n

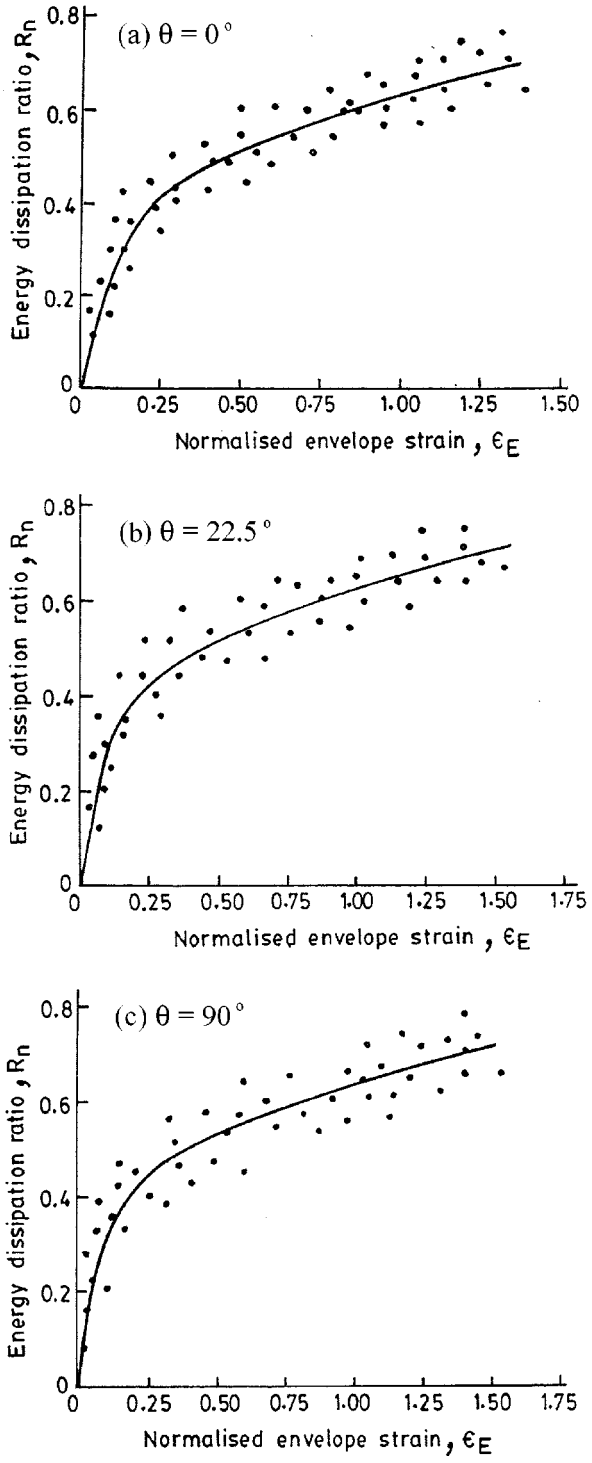

Fig. 13(a, b, c) R_n versus envelope strain

where,
R_n = energy dissipation ratio
Ln = natural logarithm
ε_E = normalised envelope strain
α_1, β_1 = equation's constants

The values of α_1 and β_1 were determined from test data and they were found to be 0.40, 0.39 and 0.37, and 0.93, 0.92 and 0.92 for bed joint inclination equals to 0^o, 22.5^o and 90^o respectively. The degree of fit of the empirical expression with test data was indicated by the correlation index, i_c which was 0.91 for all three cases of loading. In general, the variation of energy dissipation ratio, R_n with respect to the envelope strain exhibits three typical ranges with distinct trends: an initial linear portion with a high rate of increase in R_n and low rate of increase in strain followed by a transitory non - linear portion and, finally a relatively approximate linear portion with slower rate of increase in R_n and faster rate of increase in strain ratio. A linear equation may be used to approximate the relationship between R_n and ε_E up to an envelope strain ratio of approximately equal to 0.2 for all three cases of loading. The limiting strain ratio corresponds to stress ratios of approximately equal to 0.40, 0.38 and 0.35 for bed joint inclinations equals to 0^o, 22.5^o and 90^o to the horizontal respectively. The corresponding stress ratio values may be regarded as the elastic limit for the material. Thereafter, the energy dissipation ratio increases at a slower rate up to an envelope strain ratio approximately equal to 1.4. The high rate of increase of R_n in the initial stage and the slower rate of increase of R_n at later stage may be attributed to differences in the formation and size of cracks in the two stages.

Fig. 14 shows the experimentally observed variation in the energy dissipation ratio, R_n versus the plastic strain ratio, ε_r for the three cases of loading. The experimental variable may be represented by the following semi - empirical relationship:

For $\theta = 0^o$,

$$R_n = \frac{1}{\beta_2^2}\varepsilon_r^{\alpha_2}\ln(\varepsilon_r^{\alpha_2} + 1.15) \tag{4a}$$

For $\theta = 22.5^o$,

$$R_n = \frac{1}{\beta_2^2}\varepsilon_r^{\alpha_2}\ln(\varepsilon_r^{\alpha_2} + 1.15) \tag{4b}$$

For $\theta = 90^o$,

$$R_n = \frac{1}{\beta_2^2}\varepsilon_r^{\alpha_2}\ln(\varepsilon_r^{\alpha_2} + 1.20) \tag{4c}$$

where,
R_n = energy dissipation ratio
ln = natural logarithm
ε_r = plastic strain ratio
α_2, β_2 = equation's constants.

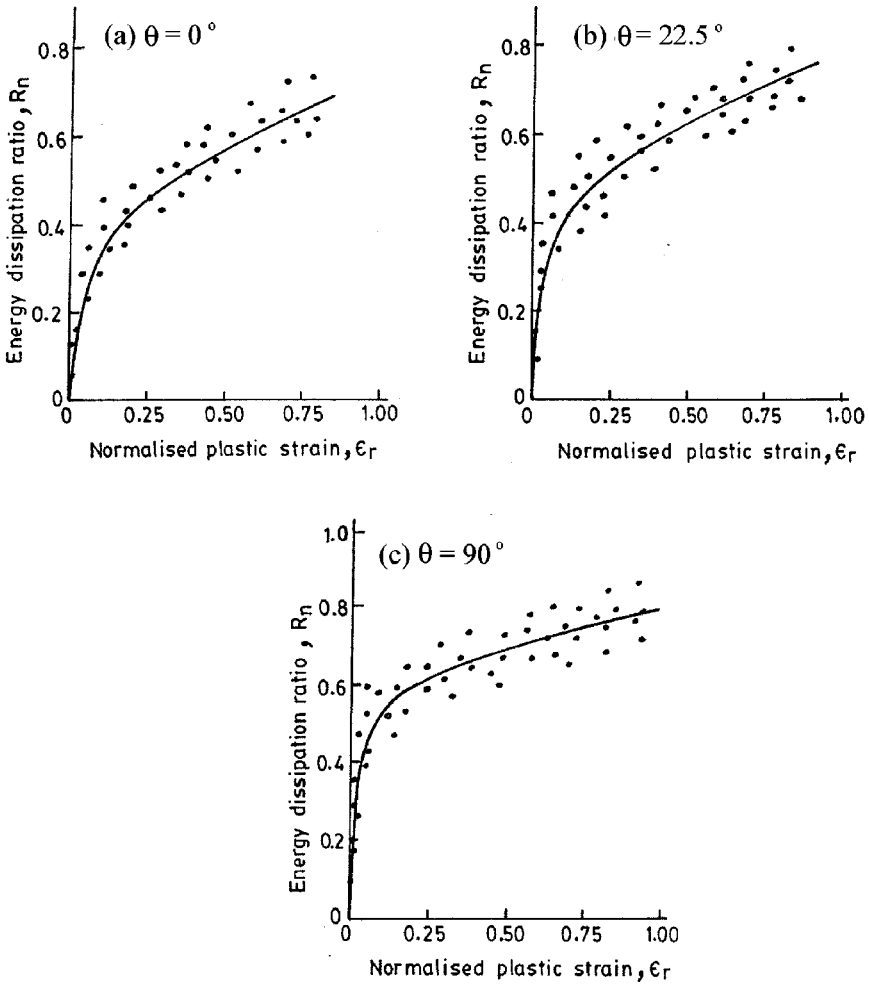

Fig. 14(a, b, c) R_n versus plastic strain

The values of α_2 and b_2 are determined from test data. For bed joint inclination equals to 0^o, α_2 and β_2 are equal to 0.20 and 1.05. Similarly for bed joint inclinations equals to 22.5^o and 90^o, α_2 and β_2 are 0.15 and 0.10, and 1.025 and 1.0 respectively. It provided an index of correlation with test data of 0.94, 0.91 and 0.89 for 0^o, 22.5^o and 90^o respectively.

It may be noted that the relationship between R_n and ε_r is bilinear and similar to that between R_n and ε_E behaviour. A higher rate of increase in R_n is observed at early stages of loading wherein only micro - cracks form with insignificant accumulation of plastic strain. A slower increase in R_n with faster increase in ε_r at later stages of loading reflects the growing and widening of cracks and thus faster accumulation of plastic strain.

An approximately linear relationship exist between R_n and ε_r up to a plastic strain ratio, ε_r of approximately 0.14, 0.11, 0.08 for bed joint inclinations of 0^o, 22.5^o and 90^o respectively. The limiting values of plastic strain demarcate the linear range of behaviour on the R_n - ε_r curves beyond which material strength begins to deteriorate.

4. Conclusions

This paper presents the test results on the experimental behaviour of calcium silicate brick masonry models under cyclic uniaxial compression. Five loading directions comprising 0^o, 22.5^o, 45^o, 67.5^o and 90^o were considered. An envelope stress - strain curves, a common point curves and stability point curves were obtained for various test conditions. Mathematical expressions were proposed for the three stress - strain curves. The stress - strain hysteresis of the cyclic loading was used to evaluate the energy dissipation characteristics of calcium silicate brick masonry. The energy dissipation ratio, R_n was plotted with respect to normalised envelope strain and normalised plastic strain. These plots exhibited bilinear behaviour with an initial linear range that shows a high rate of increase in R_n followed by an intermediate short non - linear zone of transition and then a relatively linear portion that displays a relatively slower rate of increase in R_n and a higher increase in strain than the initial portion. The relation between R_n and ε_r can be used to identify the limiting point in the loading history that signifies the on set of strength degradation.

References

Alshebani, M.M. and Sinha, S.N. (1999), "Energy dissipation of masonry under cyclic biaxial compression", *Int. Conf. on Structures Under Shock and Impact - VI*, University of Cambridge, London, 427-436.

Atkinson, R.H. and Noland, J.L. (1983), "A proposed failure theory for brick masonry in compression", *Proc. 3rd. Canadian Masonry Symp.*, Edmonton, 5.1-5.17.

Banon, H., Biggs, J.M. and Irvine, H.M. (1981), "Seismic damage in reinforced concrete frames", *J. Struct. Div.*, ASCE, **107**(ST9), 1713-1729.

Bertero, V.V. and Popov, E.P. (1977), "Seismic behaviour of ductile moment resisting reinforced concrete frames", *Reinforced Concrete Structures in Seismic Zones*, SP-53, American Concrete Institute, Detroit, 247-291.

Chen, S-W. J., Hidalgo, P.A., Mayes, R.L., Clough, R.W., and McNiven, H.D. (1978), "Cyclic loading tests of masonry single piers, Volume 2 - Height to width ratio of 1", *EERC Report No. 78/28*, University of California, Berkeley.

Darwin, D. and Nmai, C.K. (1986), "Energy dissipation in RC beams under cyclic load", *J. Struct. Div.*, ASCE, **112**(8), 1829-1846.

Gosain, N.K., Brown, R.H. and Jirsa, J.O. (1977), "Shear requirements for load reversals on RC members", *J. Struct. Div.*, ASCE, **103**(ST7), 1461-1476.

Hidalgo, P.A., Mayes, R.L., McNiven, H.D. and Clough, R.W. (1978), "Cyclic loading tests of masonry single piers, Vol. 1 - Height to width ratio of 0.2", *EERC Report No. 78/27*, University of California, Berkeley.

Hwang, T.H. and Scribner, C.F. (1984), "R/C member cyclic response during various loadings", *J. Struct. Div.*, ASCE, **110**(3), 477-489.

Khoo, C.L. and Hendry, A.W. (1973), "A failure criterion for brickwork in axial compression", *Proc. of the Third Int. Brick Masonry Conf.*, Essen, (ed. L. Foertig and K. Gobel), 139-45.

Mayes, R.L. and Clough, R.W. (1975), "State-of-the-art in seismic strength of masonry - An evaluation and review", *EERC Report No. 75 - 21*, University of California, Berkeley.

Mengi, Y. and McNiven, H.D. (1989), "A mathematical model for the in-plane non-linear earthquake behaviour of unreinforced masonry walls. Part 1: Experiments and proposed model", *Earthq. Engrg. Struct. Dyn.*, **18**, 233-247.

Naraine, K. and Sinha, S. (1989), "Behaviour of brick masonry under cyclic compressive loading", *J. Struct. Engng.* **115**(6), 1432-1445.

Popov, E.P. (1968), *Introduction to Mechanics of Solids*, Prentice-Hall, Inc., Englewood Cliffs, N.J.

Shing, P., Noland, J., Spaeh, H. and Klamerus, E. (1987), "Inelastic behaviour of masonry wall panels under in-plane cyclic loads", *Proc. 4th Nth. Am. Mas. Conf.*, Los Angeles, California, 42.1-42.14.

Sinha, S.N. and Naraine, K. (1991), "Energy dissipation in brick masonry under cyclic biaxial compressive loading", *Proc. of Inst. of Civil Engrs.*, Part 2, 173-181.

Warren, D. and Lenczner, D. (1981), "Creep-time function for single leaf brickwork", *Int. J. Masonry Constr.*, **2**(1), 13-20.

Notation

e	: Axial strain
e_c	: Compressive strain
e_m	: Axial strain at peak stress
e_r	: Plastic (residual) strain
f	: Stress
f_c	: Compressive stress
f_m	: Failure (peak stress)
i_c	: Index of correlation
L_n	: Natural logarithm
R_n	: Energy dissipation ratio
ε	: Non - dimensional axial strain
ε_E	: Non - dimensional envelope strain
ε_C	: Non - dimensional common point strain
ε_S	: Non - dimensional stability point strain
ε_r	: Non - dimensional plastic (residual) strain
σ	: Non - dimensional axial stress
σ_{peak}	: Maximum stress level
σ_s	: Non - dimensional stress at the peak of stability point curve
θ	: Angle between horizontal and the bed joint
α_1, β_1, α_2 and β_2	: Equation's constant